

Characterization of the Lick Adaptive Optics Point Spread Function

Szymon Gladysz^{ab}, Julian C. Christou^a, Michael Redfern^b

^a Center for Adaptive Optics, University of California, Santa Cruz, CA 95064, USA.

^b Department of Experimental Physics, National University of Ireland, Galway, Ireland

ABSTRACT

We have investigated both the temporal and spatial structure of the point spread function (PSF) produced by the Lick Observatory adaptive optics (AO) system using the FastSub readout mode of the IRCAL camera using short-exposure images with exposure times of 22ms at a frame rate of ~ 20 Hz suitable for “freezing” the compensation under typical *K*-band observing conditions. These short exposures are a useful diagnostic tool for determining the system performance and permit measurement of the instantaneous Strehl ratio. Data taken from a number of observing runs, spanning over four months, show the underlying morphology of the PSF to be very stable with instantaneous Strehl ratios varying from $\sim 20\%$ – 70% in NGS mode. Estimates of the instantaneous Strehl distribution have also been obtained from which we have determined the probability density function for the distribution of the instantaneous Strehl ratios.

Keywords: adaptive optics, system performance, Strehl ratio, natural guide stars

1. INTRODUCTION

In this paper we present measurements of the performance of the Lick Observatory natural guide star (NGS) adaptive optics (AO) system. In order to investigate the performance of the high order system we took *K*-band short exposure images, essentially freezing the compensation, so that residual image motion due to the tip-tilt correction did not affect our analysis. The residual image motion from some of the data reported here has been used to investigate the telescope tracking¹.

Baldwin et al. have shown that selection of the best short-exposure speckle images without AO can significantly improve final image quality². This “lucky exposures” imaging prompted our study of the closed-loop AO short-exposure images to investigate how effective this approach would be for closed-loop AO imaging given that AO systems stabilize the image quality. We have used the Strehl ratio, S , of the closed-loop short-exposure images as an image quality metric. This has allowed us to investigate the temporal distribution of the instantaneous Strehl ratio and to compare it to models allowing us to develop a probability density function (PDF) of the Strehl ratios in this mode of operation. This data has also allowed us to look at the temporal stability of the Lick AO point spread function (PSF), not only on short time scales but over a period of months as well.

2. OBSERVATIONS AND DATA ANALYSIS

We observed a number of single stars during a sequence of natural guide star (NGS) engineering nights in the latter half of 2005. The observing details are given in Table 1. All data were taken using the AO system on the Lick Observatory 3m Shane Telescope³. Closed loop images for these objects were obtained using the high-speed sub-array mode (FastSub) with a size of 64×64 pixels⁴ of the 256×256 pixel IRCAL camera⁵. This corresponds to field size of 4.864×4.864 arcseconds, assuming the standard image scale of 0.076 arcseconds/pixel. Recent measurements show the image scale to have small scale variations across the detector⁶ but these can be neglected for the analysis performed here in that the sub-array was generally in the same position on the full array. The FastSub mode permits image sizes of both 64×64 pixels and 32×32 pixels and the larger one was chosen to ensure that the uncompensated seeing halo was captured which is necessary for the photometric calibration required to compute the Strehl ratio. The sub-array measurements were captured with typical exposure times of 22ms although some were obtained at a longer exposure time of 57ms. The readout time of the 64×64 pixel sub-array is 30ms for 16 resets giving cycle times of 52ms (~ 20 Hz) and 87ms (~ 11.5 Hz) for the two exposure times. Each data set comprises at least ten thousand images taken in ten groups of one

thousand, the maximum currently possible in burst mode for this size sub-array. In addition a series of one thousand sky frames were obtained 20" away from each object before and after the each object observation. All data were obtained in the two-micron band where the diffraction-limit is 151 mas so that the data is effectively Nyquist sampled and the correlation time is longer. The observations were made close to the zenith and using the highest possible closed-loop frame rate. Seeing estimates were obtained from the power spectra of the AO closed-loop operation.

Table 1: Point Source Observations

PSF No.	USNO Catalogue ID	ZD ($^{\circ}$: ' : ")	Date (UT)	Filter ($2\mu\text{m}$)	m_l	t_{sub} (ms)	AO Frame Rate (Hz)	r_0 (cm)
1	3124-02056-1	11:56:34	2005-07-26	Br_{γ}	6.06	22	500	18.9
2	3124-01860-1	17:14:15	2005-07-26	K_s	7.55	22	500	17.8
3	3106-02121-1	06:41:44	2005-08-19	K_s	6.01	22	500	21.8
4	3106-01230-1	11:42:02	2005-08-19	K_s	8.96	22	100	20.2
5	3124-02056-1	04:40:09	2005-08-19	Br_{γ}	6.06	22	500	24.1
6	3216-01890-1	13:52:45	2005-08-19	K_s	6.14	22	500	25.7
7	2783-00925-1	03:37:14	2005-08-19	Br_{γ}	5.95	22	500	21.6
8	2783-01072-1	09:00:14	2005-08-19	K_s	6.90	57	500	23.0
9	1297-0486637	06:24:10	2005-10-11	K_s	9.00	22	55	18.0
10	1297-0486637	09:07:16	2005-10-11	K_s	9.00	22	55	14.3
11	2850-00537-1	02:35:37	2005-10-13	K_s	6.62	22	500	16.0
12	2850-00537-1	05:11:02	2005-10-13	K_s	6.62	22	500	
13	2850-00537-1	07:23:56	2005-10-13	K_s	6.62	22	500	
14	2850-00537-1	12:33:46	2005-10-13	K_s	6.62	22	500	18.8
15	2850-00537-1	15:02:09	2005-10-13	K_s	6.62	22	500	
16	2850-00537-1	17:23:02	2005-10-13	K_s	6.62	22	500	
17	3216-02164-1	00:55:24	2005-11-19	K_s	7.43	57	500	
18	3216-02164-1	04:06:41	2005-11-19	K_s	7.43	57	500	
19	3219-03305-1	11:42:02	2005-11-19	K_s	6.26	22	500	19.0
20	3219-03305-1	14:58:47	2005-11-19	K_s	6.26	22	500	
21	2820-01519-1	14:50:11	2005-11-19	K_s	6.23	22	500	12.0
22	2820-01519-1	11:48:54	2005-11-19	K_s	6.23	22	500	17.8
23	2816-00766-1	02:01:22	2005-11-19	K_s	7.75	57	350	
		Br_{γ} (2.167;0.020 μm).			K_s (2.150;0.320)			

Each frame from the 1000 frame data set was flat-field corrected and sky-subtracted and then processed with a peak-tracking algorithm. This algorithm locates the peak in each of the images and locates its sub-pixel value by computing the centroid of a 3×3 pixel box centered on the peak pixel. This box is big enough to contain the diffraction-limited core of the AO PSF. Each frame is then shifted by computing its Fourier transform and applying a slope to the Fourier phases corresponding to the offset of the sub-pixel peak location from the frame center, i.e. pixel (33,33), and then computing the inverse Fourier transform. The procedure is repeated until a tolerance of 0.02 pixels (~ 2 mas) is reached. This represents Fourier interpolation and retains the Fourier structure of the data unlike other interpolation procedures such as the bi-cubic spline. Besides computing the sub-pixel peak location and the interpolated peak value, the algorithm also saves the peak-shifted version for each frame as well as the co-added raw frames, i.e. the long exposure, and the co-added shifted frames, i.e. the shift-and-add (SAA) image. For this analysis the latter 950 frames were used as the first 1000 were contaminated by a variable bias due to the chip readout.

2.1 Strehl Ratio Measurements

Strehl ratio computation is problematic⁷. Benefiting from the advice given in this paper we have carefully computed the Strehl ratios as follows. An ideal PSF for the telescope is computed numerically at an $8\times$ higher spatial resolution than the Nyquist-sampled data. This is done by computing an annular aperture at the corresponding pupil-plane scale using "soft" edges, i.e. by using fractional pixel intensity values when the edge of the pupil is not fully sampled by a pixel. From Fourier optics the PSF is simply the power spectrum of this annulus. The effect of pixel binning is then simulated by binning the PSF from the original 512×512 pixel size to the final 64×64 pixel size keeping the same field size. This has been found to yield significantly more accurate Strehl ratios when comparing the measured PSFs to either numerically or analytically derived ones PSFs generated with the correct sampling but without the binning effects accounted for.

The SAA images were found to have a small residual bias, typically less than a count, which was subtracted. This residual bias was estimated from the intensity histogram of the SAA image. The additive noise in the image showed as a Gaussian with a mean close to, but not at, zero. The ideal PSF and SAA image were then normalized to have the same power within a radius of 25 pixels (1.9 arcseconds). This aperture was determined by investigating the images to ascertain when the noise floor was reached. The ratio of the normalized SAA images to that of the normalized ideal PSF then gives the Strehl ratio (S) for each SAA image. The peak value of the shift-and-add image and its corresponding Strehl ratio yields a correction factor which, when applied to the peak values of the individual frames used to generate the SAA image, gives their individual Strehl ratios. Furthermore, the variance in these correction factors (σ_c^2) yields an uncertainty in the Strehl ratio determination for the shift-and-add images for a particular data set. The advantage of computing the Strehl ratio in this manner is that, by using the shift-and-add images, it is computed on a significantly higher SNR ($31\times$) image than for an individual frame. Furthermore, the shift-and-add images ensure that the peak value is centered on a single pixel. This is not necessarily the case for the long exposures and their Strehl ratios were computed after applying the same Fourier shift procedure to place the image core on a single pixel as for individual frames.

Table 2: Mean Instantaneous Strehl Ratio

No.	Object	S (%)	σ_c	σ
1	3124-02056-1	48.1	0.4	1.8
2	3124-01860-1	51.1	0.6	1.8
6	3216-01890-1	51.9	0.1	1.2
8	2783-01072-1	48.9	0.2	1.5
9	1297-0486637			
11	2850-00537-1	48.5	0.3	3.6
12	2850-00537-1	37.9	0.5	3.6
13	2850-00537-1	41.8	0.4	2.1
14	2850-00537-1	33.5	0.1	5.4
15	2850-00537-1	44.3	0.2	2.8
16	2850-00537-1	43.9	0.8	5.2
17	3216-02164-1	46.6	0.4	3.3
18	3216-02164-1	47.1	0.3	2.6
19	3219-03305-1	45.1	0.3	2.9
20	3219-03305-1	44.5	0.2	1.5
21	2820-01519-1	37.6	0.8	5.6
22	2820-01519-1	36.6	0.6	4.3
23	2816-00766-1	43.5	0.6	3.6

Table 2 gives the mean Strehl ratios for 10,000 frame data sets for the stars given in Table 1, hence the different subsets for the different objects. Figure 1 shows the corresponding SAA images. These values represent the mean Strehl ratios for the data sets based on the SAA images as discussed above. The dispersion of the Strehl ratio/peak conversion factors is given by the fourth column σ_c whereas the dispersion in Strehl ratio values per data set is given in the fifth column, σ . The uncertainty in the Strehl ratio computation is typically $\sigma_c \sim 1\%$ of the mean whereas the dispersions are much greater $\sigma \sim 10\%$ of the mean indicating that we are measuring real changes in the AO compensation. These mean Strehl ratios range from a low of 33% to a high of 51.9% with a mean value of $\sim 44\%$.

These measurements are some of the first high-speed measurements of Strehl ratio in a closed loop AO system and allow investigation of the instantaneous compensation. The difference between the two extremes of the AO compensation for PSFs 1, 2, 6 & 8 is shown in Figure 2 which compares the best and worst compensated frame for each data set. The best frame clearly shows the first ring of the Airy pattern whereas the worst frames are beginning to show secondary peaks and strong pinned speckles at the location of the first Airy ring. It is also worth noting that the residual speckle structure seen in the best compensated images is consistent across the four objects even though the two pairs of data were observed about a month apart.

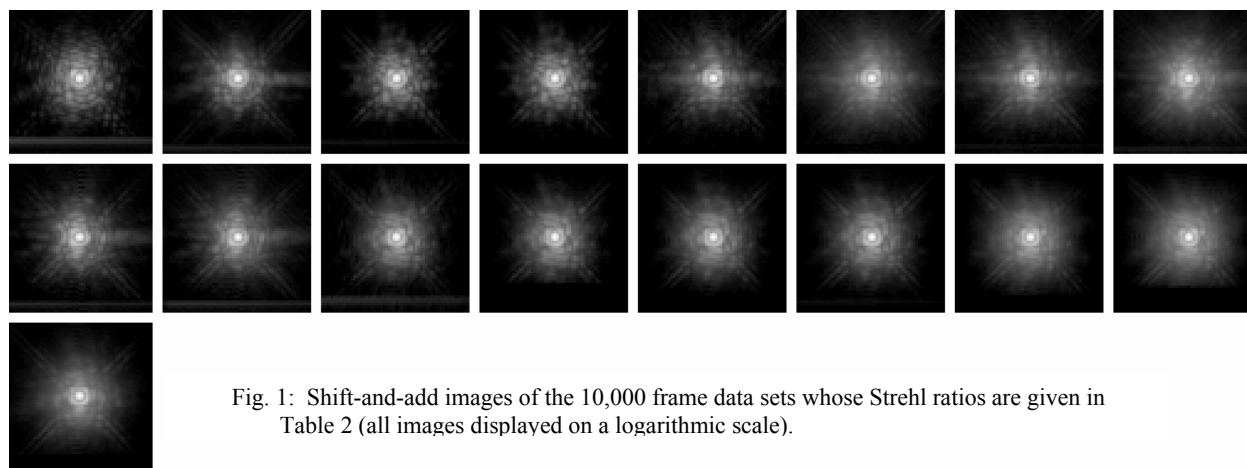


Fig. 1: Shift-and-add images of the 10,000 frame data sets whose Strehl ratios are given in Table 2 (all images displayed on a logarithmic scale).

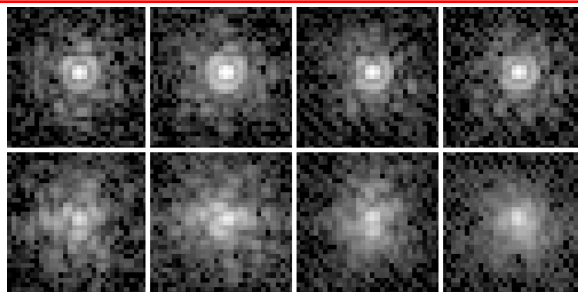


Fig. 2: Best (top) and worst (bottom) compensated frames for PSFs 1, 2, 6 & 8 (left-to-right). The best Strehl ratios are 66%, 64%, 68%, and 64% respectively and the worst are 19%, 26%, 25% and 26%. (All images displayed on a logarithmic scale, FoV = 2.3 arcseconds).

Figure 3 shows the instantaneous Strehl ratio variations for the data subsets in Table 2. As can be seen there are some strong variations in Strehl ratio and hence the compensation over different temporal scales. This is true even when the correction is relatively stable (stationary) such as for PSFs 1, 2, 6 and 8. As can be seen, there is a large variation in the Strehl ratio values ranging from highs $\sim 70\%$ to lows $\sim 20\%$ over time scales \sim minutes or less. The 60,000 measurements for (PSFs 11–16) show the Strehl ratio to be changing on relatively fast time scales with a variable mean and large departures. This is also seen for PSFs 17–23.

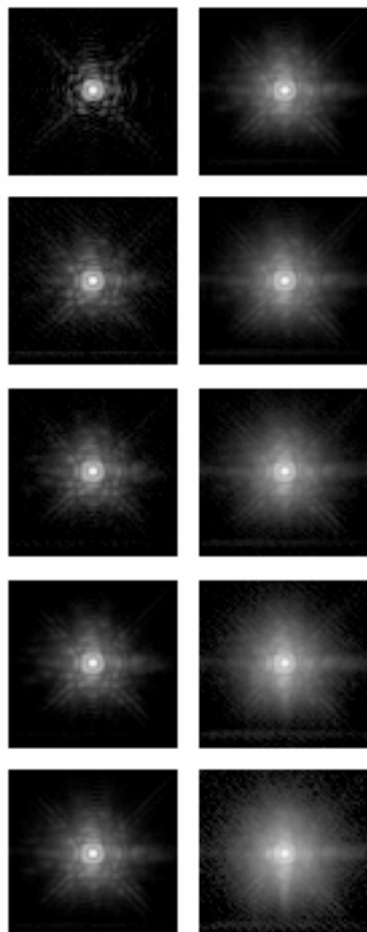


Fig. 4: (Left) Mean PSFs for the Strehl ratio selected frames from the 60000 frames data set for star 6 with Strehl ratio decreasing from top-to-bottom and left-to-right. The top left image is the internal fiber source with a Strehl ratio of 78%.

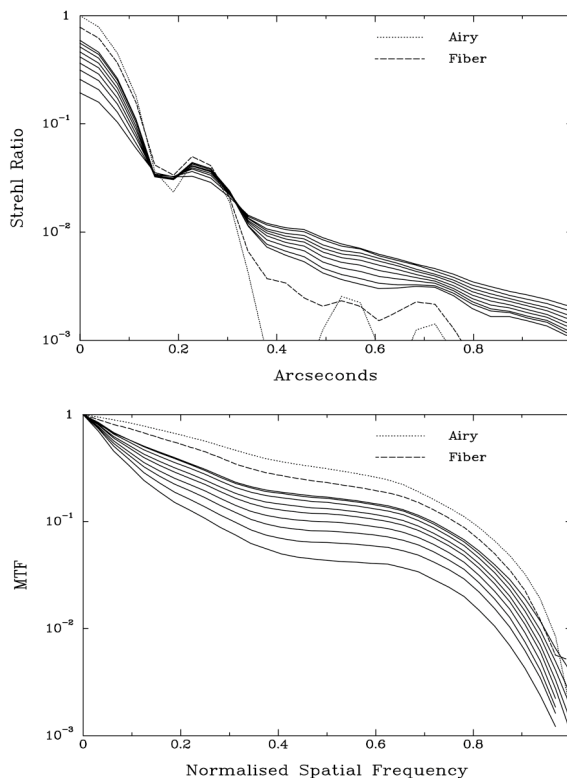


Fig. 5: (Above) Azimuthally averaged radial profiles of the PSFs in Fig. 4 (top) and the corresponding MTFs (bottom). These are compared to the ideal PSF (Airy) and the fiber source.

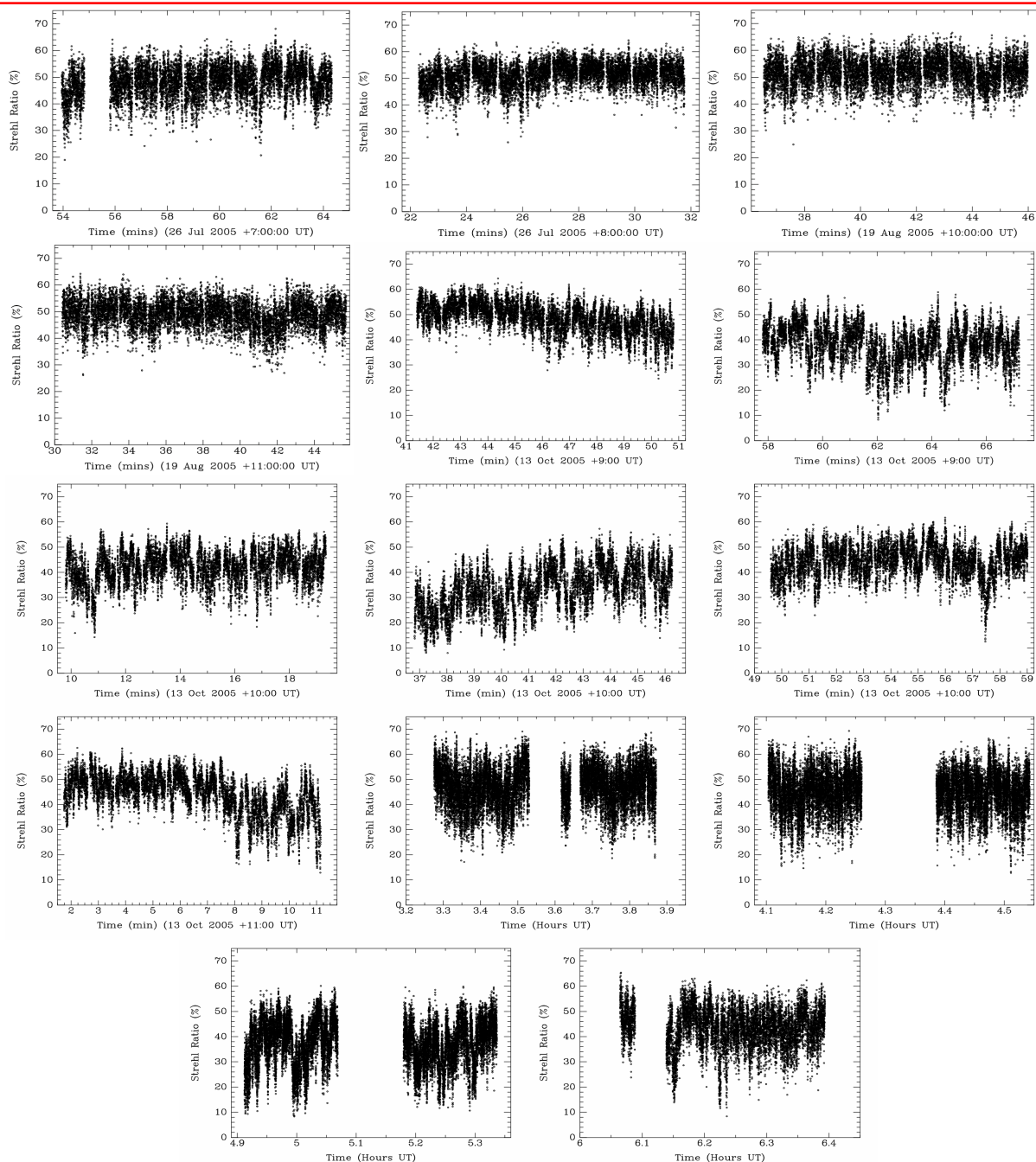


Fig. 3: Instantaneous Strehl ratios for the data sets in Table 2 in order from left-to-right and top-to-bottom. The final four plots show 20,000 frame measurements.

The large Strehl ratio variation over 60,000 frames for 2850-00537-1 permits a selection of the data according to Strehl ratio in order to compare the mean PSF for different levels of compensation for the Lick AO system. This is shown in Figure 4. The data was split into nine separate bins with mean Strehl ratios of 59%, 56%, 51%, 46%, 42%, 36%, 31%, 26% and 19%. These were compared to the image of the internal calibration source which had a Strehl ratio of 78%. As can be seen, the PSF behaves as expected in that the core diminishes in intensity compared with the wings of the PSF as the mean Strehl decreases. In all cases, the first Airy ring is clearly visible but its contrast is severely reduced as the compensation decreases. Figure 5 shows the azimuthally averaged radial profiles for the PSFs and the corresponding

MTFs respectively. The PSF radial profiles show that the best contrast obtainable from the Lick AO system is ~ 7 magnitudes at $0.5''$ from the image core with the internal calibration source. Under the best atmospheric conditions, i.e. $S \sim 60\%$ this decreases to ~ 6 magnitudes and under the worst conditions of $S \sim 20\%$ to ~ 5 magnitudes.

The measurements of the fiber source indicate that the best possible Strehl from the Lick AO system is $S \sim 80\%$. Repeated measurements are very consistent from month to month, not only in the value of the Strehl but also in the structure of the PSF. This is illustrated in Figure 6. Notice the high spatial frequency residual structure in the PSF. We are currently investigating why we cannot achieve higher Strehl ratios than this.

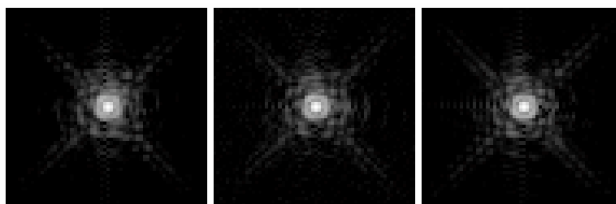


Fig. 6: Three separate images of the internal calibration source of the Lick AO system measured in September, October and November 2005. Note the consistency in the residual speckle structure in the three PSFs. The Strehl ratios are 75%, 80% and 75% respectively. (All images displayed on a logarithmic scale).

2.2 Strehl Ratio Distribution

The histograms of the instantaneous Strehl ratios for the four quasi-stationary observations for PSFs 1, 2, 6 & 8 are shown in Figure 7. All four show a negatively-skewed distribution with an excess of low-Strehl ratio values. So why is this? In case of no AO correction speckle intensity statistics obey exponential distribution. For higher orders of wavefront coherence, a modified Rician distribution⁸ has been employed for the description of the resulting intensity statistics. The Rician probability density function (PDF) has also been used as a model for off-axis intensity fluctuations in case of partial^{9,10} and very high¹¹ AO correction. It has recently been tested using short-exposure data (sampling period of 14.5 ms) from the Lick Observatory⁴ and a good agreement was found but only locations outside image core were investigated. All afore-mentioned distributions are positively skewed.

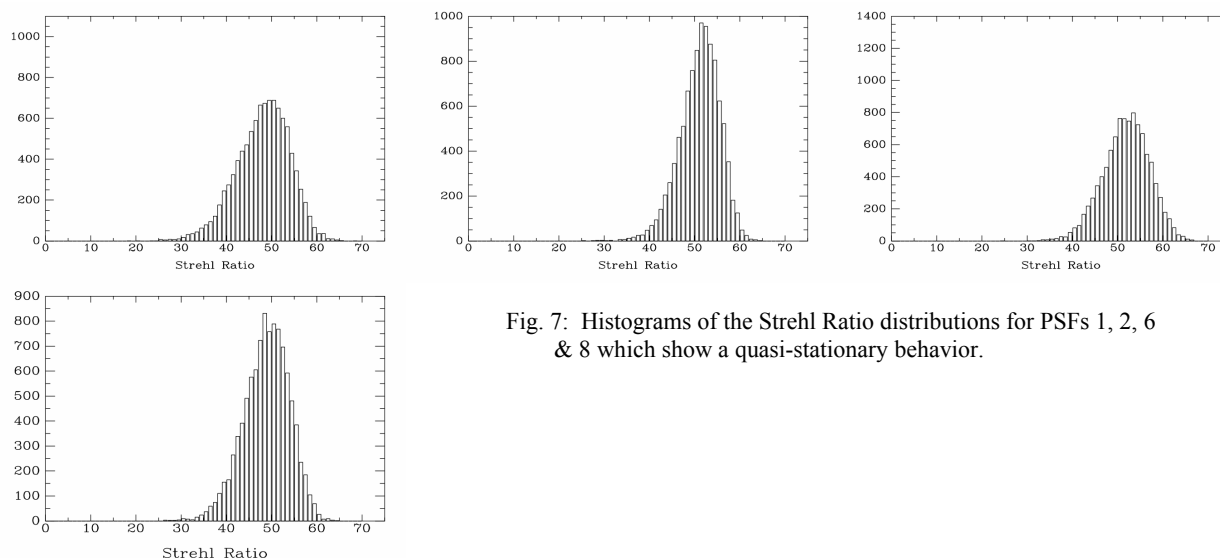


Fig. 7: Histograms of the Strehl Ratio distributions for PSFs 1, 2, 6 & 8 which show a quasi-stationary behavior.

In order to understand these negatively-skewed distributions, we consider the PDF of the closed-loop instantaneous Strehl ratio measurements.

2.3 Probability Density Function of the Instantaneous Strehl ratio

The PDF of the instantaneous Strehl ratio is related to the PDFs of random variables which determine the system performance and the state of the turbulent atmosphere. The Strehl ratio is related to the residual wavefront variance by the extended Marechal approximation:

$$S = e^{-\sigma^2} \quad \text{for} \quad \sigma^2 = \sigma_F^2 + \sigma_{BW}^2 + \sigma_{TD}^2 \quad (1)$$

where σ_F^2 is the fitting error, σ_{BW}^2 is the bandwidth error and σ_{TD}^2 is the time delay error. These wavefront errors can be expressed as

$$\sigma_F^2 = \mu \cdot \left(\frac{d}{r_0}\right)^{5/3} \quad \text{and} \quad \sigma_{BW}^2 = \kappa \cdot \left(\frac{f_G}{f_s}\right)^{5/3} \quad \text{and} \quad \sigma_{TD}^2 = 28.4 \cdot (\tau_s f_G)^{5/3} \quad (2)$$

where d is the actuator spacing (0.5m), $\mu \sim 0.27$ is the fitting error coefficient¹², $f_G \sim v / r_0$ is the Greenwood frequency assuming single turbulent layer moving at speed v , $\kappa = 1.0$ is a coefficient depending on the spectral shape of the control loop transfer function¹³ and τ_s is the reciprocal of AO frame rate. All three errors share a common dependence on $r_0^{-5/3}$. The mean wind speed at Lick is estimated at $\sim 13\text{m/s}$ using previous measurements^{12,14} of r_0 and f_G .

Thus

$$S = \exp(-A r_0^{-5/3}) \quad \text{where} \quad A = 0.27 d^{5/3} + \left(0.427 \frac{v}{f_s}\right)^{5/3} + 28.4 (\tau_s \cdot 0.427 v)^{5/3} \quad (3)$$

The probability that a random variable S (Strehl ratio) will take on a value s or smaller is given as

$$P\{S \leq s\} = P\{\exp(-A \cdot R_0^{-5/3}) \leq s\} = P\left\{R_0 \leq \left(-\frac{\ln s}{A}\right)^{-3/5}\right\} \quad \text{and} \quad F_S(s) = F_{R_0}\left(\left(-\frac{\ln s}{A}\right)^{-3/5}\right)$$

where $F_S(s)$ is the cumulative density function and R_0 is a random variable with possible values r_0 .

The PDF is expressed as $f_S(s) = f_{R_0}\left(\left(-\frac{\ln s}{A}\right)^{-3/5}\right) \cdot |J|$ where $|J|$ is equal to the absolute value of the Jacobian of the transformation $r_0 = \left(-\frac{\ln s}{A}\right)^{-3/5}$ so that

$$f_S(s) = f_{R_0}\left(\left(-\frac{\ln s}{A}\right)^{-3/5}\right) \cdot \left(-\frac{3}{5}\left(-\frac{\ln s}{A}\right)^{-8/5}\right) \cdot \left(-\frac{1}{A s}\right) \quad (4)$$

where s is always positive. r_0 has been observed to follow the log-normal distribution^{14,15} so that

$$f_{R_0}(r_0) = \frac{1}{\sigma \sqrt{2\pi}(r_0 - \theta)} \exp\left(-\frac{(\ln(r_0 - \theta) - \zeta)^2}{2\sigma^2}\right) \quad (5)$$

where θ is the threshold parameter of the distribution, $\theta < \min(r_0)$, ζ is the scale parameter, $e^\zeta = \text{median } r_0$ and σ is the shape parameter, $\sigma > 0$. Combining (4) and (5) yields

$$f_S(s) = \frac{C}{s} s'^{8/3} (s' - \theta) \frac{2\zeta - \ln(s' - \theta) - 2\sigma^2}{2\sigma^2} \quad (6)$$

where $C = 3 \exp(-\zeta^2/2\sigma^2)/5A\sigma\sqrt{2\pi}$ and $s' = (-\ln s/A)^{-3/5}$

which has a negative skewness as seen in the Strehl ratios histograms. It should also be noted that a similar procedure based on the Gaussian PDF for r_0 produces again a negatively-skewed PDF for the Strehl ratio. Log-normal distribution assumed earlier has been observed for *average* r_0 while we seek distribution of instantaneous r_0 . To date no such measurements have been performed.

We used the Levenberg-Marquardt least-squares method¹⁶ to fit the measured histograms along with constraints imposed on the parameters of the log-normal distribution given by equation (5). Specifically the variability of ζ is limited in the range $[\ln(r_{0min}), \ln(r_{0max})]$, where $r_{0min} = 0.5m$ and $r_{0max} = 1.35m$ are the lowest and highest expected median r_0 in K-band estimated from Table 1. An extra parameter is used to account for the power in a given histogram. The fitting routine works by minimizing the χ^2 value and provides estimates of the distribution parameters. Figure 8 shows Strehl ratio histograms and fits using (6) for PSF 3, 6 and 13.

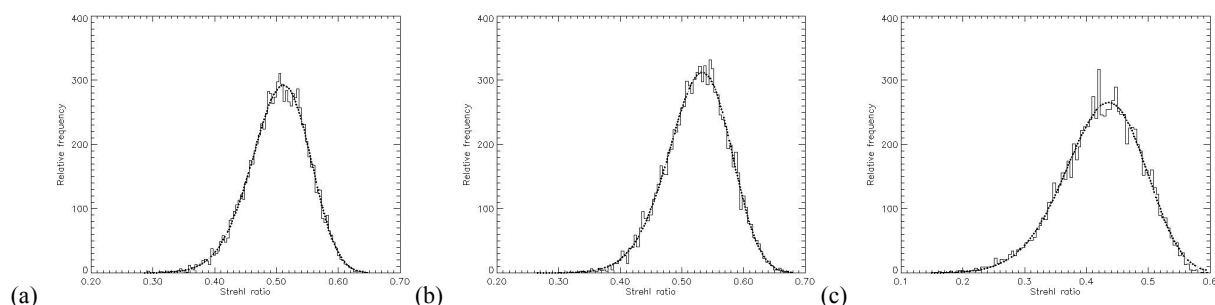


Fig. 8: Strehl ratio histograms (solid lines) and fitted PDF fits (dotted lines), (a) – PSF 3, (b) – PSF 6, (c) – PSF 13.

Figure 8 shows good fits to the measured distributions. However, not all distributions produced good fits because of either low AO frame rate or the apparent non-stationarity of the time series. The most dramatic effect can be seen for PSF 9, which has an AO frame rate of 55 Hz, which is illustrated in Figure 9. The diffraction-limited core of the SAA image is suppressed compared to the others (see Figure 1). It can be expected that when the AO frame rate is significantly lowered the resulting short exposure will be closer in resemblance to a speckle. Thus a different model for Strehl statistics should be used (positively-skewed PDF would occur²).

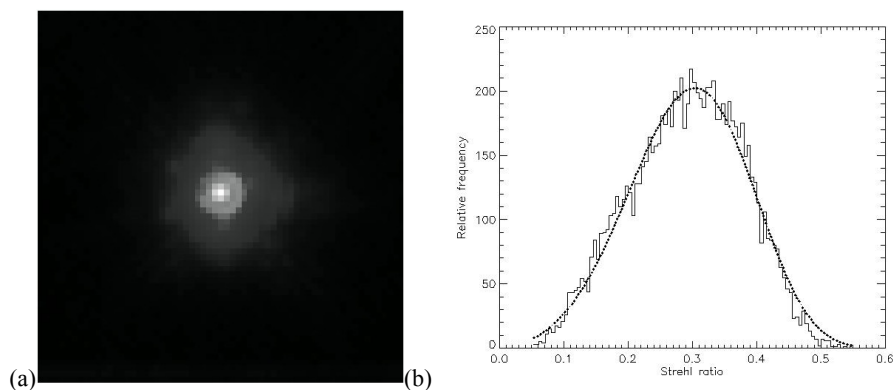


Fig. 9: PSF 9 – shift-and-add image (a) and a failed fit to the Strehl histogram (b).

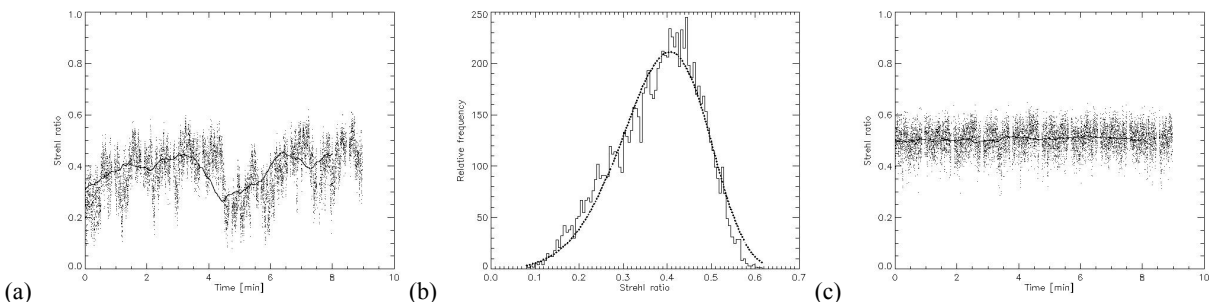


Fig. 10: Effect of non-stationarity of time series on the Strehl PDF fit (PSF 21): (a) instantaneous Strehl ratio values, dots, and moving-window average, solid line, (b) the resulting PDF fit is poor due to the excess of low values and the overall noisiness of the histogram, (c) stationary time series for comparison (PSF 3)

The stationarity of the time series was tested using a moving-window average of duration 52s (1000 data samples). High variability of this quantity implies non-stationary behavior of the data. This was encountered in eight cases. Figure 10 shows how a non-stationary time series translates into a noisy and badly defined histogram with a poor resulting fit. We compared two statistical goodness-of-fit tests, χ^2 and Kolmogorov-Smirnov¹⁷, to determine the significance of the difference between an observed distribution (histogram) and a fitted PDF. In both tests level of significance was set to 0.05. In the χ^2 test the number of degrees of freedom was reduced to account for the estimation of distribution parameters from the data. The null hypothesis that the histogram represents given PDF is rejected when the test result (p-value) is lower than 0.05. In the Kolmogorov-Smirnov test the maximum difference between the cumulative distributions is computed. This value, D_{\max} , is compared with the K-S statistic, D_α . The null hypothesis that the sample came from the assumed population is rejected when $D_{\max} > D_\alpha$. We found the χ^2 test to be more sensitive to these data especially in terms of the histogram binning. Table 3 compares the two tests.

Table 3. Results of the goodness-of-fit tests. Non-stationary time series and erroneous histograms due to low AO frame rate were excluded from this analysis. * indicate situations when exposure time was 57ms, as opposed to the usual value of 22ms. Instances of distribution rejection are indicated in italics.

	PSF number													
	1	2	3	5	6	7	8*	13	15	17*	18*	19	20	23
χ^2 p-value ($\alpha = 0.05$)	0.001	<i>8·10⁻⁵</i>	0.24	0.51	0.06	0.13	<i>7·10⁻⁴</i>	<i>5·10⁻⁵</i>	0.1	0.005	0.33	0.004	0.46	<i>10⁻⁹</i>
K-S D_{\max} ($D_\alpha = 0.014$)	0.01	0.013	0.006	0.006	0.004	0.007	0.009	0.009	0.009	0.007	0.004	0.005	0.005	0.012

3. IMAGE INTENSITY STATISTICS

The above section investigated the statistical distribution of the image quality as determined by the Strehl ratio. This is a measure of the statistics of the core of the AO compensated image. The SAA analysis also enables the statistics of the image intensity to be studied away from the image core because of the image registration removing the residual tip-tilt motion. Figure 11 shows the dependence of the intensity statistics on the position relative to the image core for PSF 6. While the on-axis intensity histogram has a negative skewness, only two pixels away from the core the histogram becomes positively skewed. The distribution becomes asymptotically Gaussian for larger distances due to readout noise.

3.4 Effect of frame correlation on the intensity distribution

PDF estimation can only be undertaken when the time series is constructed from independent and identically distributed random variables. In previous work on first-order statistical properties of AO-corrected speckles⁴ a simple method of obtaining de-correlated samples has been used. A slightly modified approach is presented here. The autocorrelation estimates of on-axis intensity (Strehl ratio) were computed within ten data cubes constituting a single observing run containing 950 usable frames each. The estimates for hundred lags (5.2 sec) were then averaged between the data cubes. The speckle correlation time is taken as the value on the abscissa corresponding to the $1/e$ decay time of the

autocorrelation¹⁸. In order to obtain better sampling across the temporal domain the autocorrelation estimate was linearly interpolated. Correlation times were found to be in the range 0.05 to 0.35 sec. The same order of magnitude was reported earlier from Lick AO data for timescales of the off-axis intensity autocorrelations⁴. Figure 12 (a) shows the computed autocorrelation for PSF 6. In this case the speckle correlation time was equal to 0.15 sec. The sampling period was 0.052 sec so every three consecutive images are considered correlated here. Frames separated in time by less than correlation time were discarded before a new histogram was generated – Figure 12 (b).

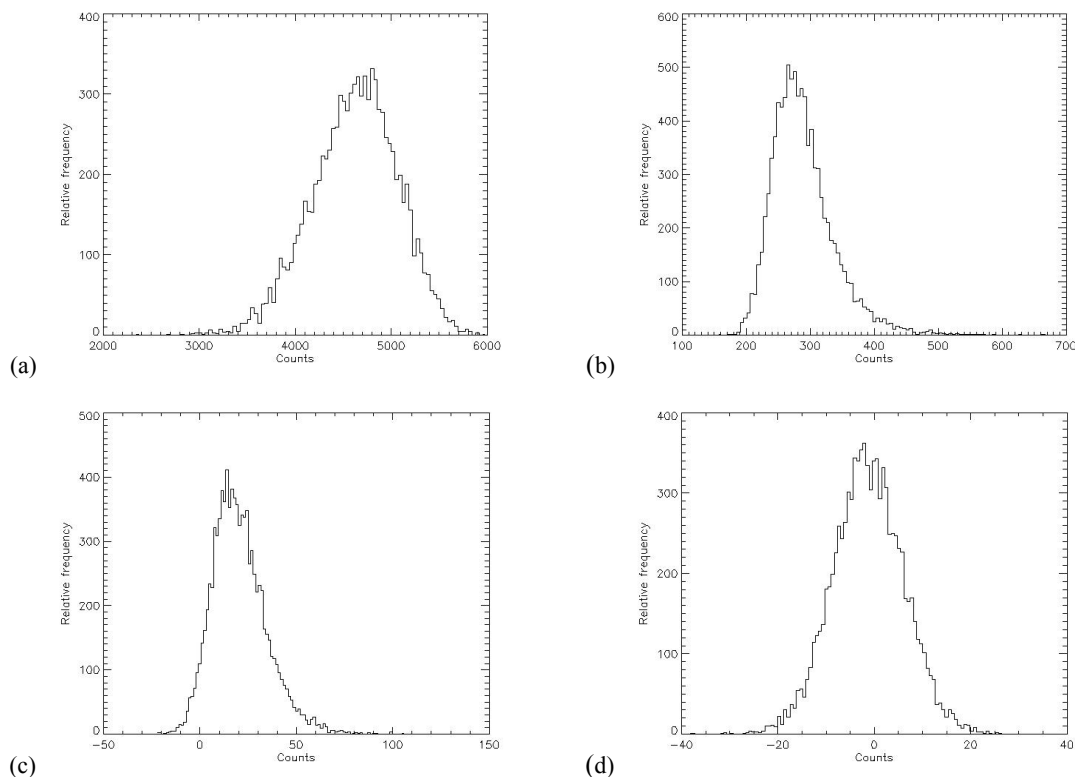


Fig. 11: Histograms of intensity for different positions in the image plane – (a) corresponds to the image core, (b) is at a radius of λ/D ($0.15''$) away, (c) is $5\lambda/D$ away and (d) is $10\lambda/D$ away (PSF 6).

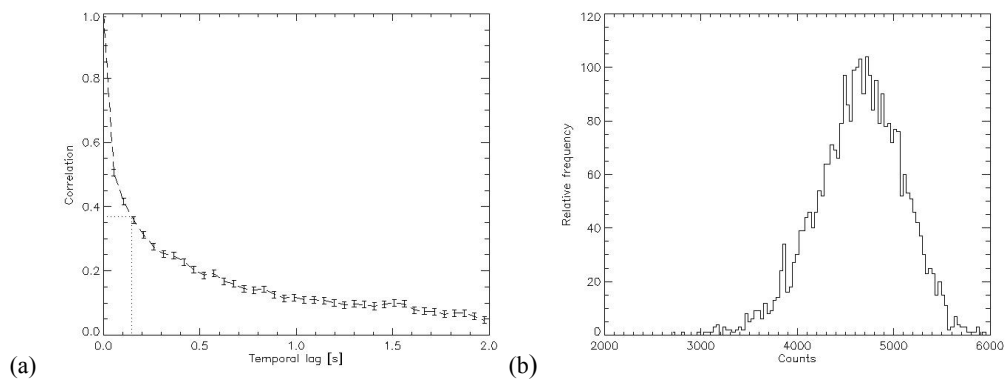


Fig. 12: (a) autocorrelation estimate for on-axis intensity (PSF 6). The e -folding value is marked with a dotted line. The error bars come from the fact that discrete autocorrelation becomes more uncertain with increasing temporal lag as less samples are averaged in the process. This error is proportional to $1/\sqrt{N}$ where N is the number of available samples for a given lag time. (b) Histogram of intensity values generated using statistically independent frames.

It can be seen that this process has not led to a new form for the intensity distribution, as expected. The only qualitative difference between Figures 11 (a) and 12 (b) is an increase in noise in the latter. It must be concluded that the distributions for on- and off-axis intensities have different functional forms.

4. SUMMARY

The Lick Observatory adaptive optics system, in natural guide star mode, provides a very stable point spread function. This is evidenced from the measurements of the internal calibration source which remains essentially constant over periods of many months. We note that the performance of the system on this internal calibration source is not optimal with Strehl ratios $\sim 80\%$ which limits the on-sky performance. The reason for this limit is not apparently clear as yet and investigations are currently planned to determine what the residual wavefront error using phase retrieval techniques.

The on-sky performance under typical seeing conditions in the K -band is $\sim 50\text{-}60\%$. However, high-speed measurements of the instantaneous Strehl ratio show that there can be strong variations ranging from $20\%\text{-}70\%$. These high-speed observations show that there are temporal fluctuations in the compensation over a variety of time scales which is the basis for a further study. In this paper we have emphasized the distribution of instantaneous Strehl ratios for quasi-stationary compensation. This study was prompted by the possible application of "Lucky Exposure"² imaging to AO speckle observations. The Strehl ratio distributions are negatively-skewed, the opposite of the positively-skewed speckle imaging case. We have explained this by computing a probability density function for the measured instantaneous Strehl ratios which depends upon the distribution of the instantaneous r_0 for the observations. This computed PDF fits well to the quasi-stationary observations assuming either a log-normal or normal distribution of r_0 . Although this analytical PDF is quite complex it serves as a validation of the experimental setup which led to the observed first-order statistics. Further observations are required to determine what the actual instantaneous r_0 values are to match with the high-speed short-exposure focal plane observations.

This analysis shows that the "lucky exposure" approach is not well suited to AO speckle imaging because of the negatively-skewed image quality distribution. However, by looking at a data set with a large range in instantaneous Strehl ratios, we have demonstrated that binning the frames according to their Strehl ratio would be advantageous in terms of signal-to-noise in the resulting image. We are investigating this aspect further. Finally we note that the AO PSF appears to contain at least two different intensity distributions for off- and on-axis locations.

ACKNOWLEDGEMENTS

This work has been supported by the National Science Foundation Science and Technology Center for Adaptive Optics, managed by the University of California at Santa Cruz under cooperative agreement No. AST-9876783 as well as COSMOGRID (Grid-enabled Computational Physics of Natural Phenomena). We would like to thank the staff of Lick Observatory, in particular Elinor Gates and Bryant Grigsby, the AO Support Scientists, for their valuable assistance with the AO system and with the data collection. In addition we'd like to thank Donald Gavel, Mike Fitzgerald, Don McGaughey, Remy Soummer, Nicholas Devaney and Jerome Sheahan for very helpful and useful discussions.

REFERENCES

1. S. Severson, J. Christou, E. Gates & Don Gavel, "Image motion control in the Lick adaptive optics system: Compensating for flexure and differential atmospheric refraction", these proceedings (2006).
2. J. E. Baldwin, R. N. Tubbs, C. D. Mackay, et al, "Diffraction-limited 800nm imaging with the 2.56m Nordic Optical Telescope", *Astron. Astrophys.* 368, L1-L4 (2001).
3. B. J. Bauman, D. T. Gavel, K. E. Waltjen, et al, "New optical design of adaptive optics system at Lick Observatory" *Proc. SPIE* 3762, 194-200 (1999).
4. M. P. Fitzgerald and J. R. Graham, "Speckle statistics in adaptively corrected images," *Astrophys.J.* 637, 541-547 (2006).

5. J.P. Lloyd, M.C. Liu, B.A. Macintosh, S.A. Sevenson, W.T. Deich, & J.R. Graham, *Proc. SPIE*, 4008, 814-821. (2000).
6. J. C. Christou and J. D. Drummond, "Measurements of Binary Stars, including two new discoveries with the Lick Observatory Adaptive Optics System", *Astron.J.*, 131, in press (2006).
7. L. C. Roberts, M. D. Perrin, F. Marchis, et al, "Is that really your Strehl ratio?" *Proc. SPIE*, 5490, 504-515 (2004).
8. J. W. Goodman, in *Laser Speckle and Related Phenomena*, ed. J. C. Dainty, Springer, 1975.
9. M. P. Cagigal and V. F. Canales, "Speckle statistics in partially corrected wave fronts," *Opt. Lett.*, 23, 1072-1074 (1998).
10. M. P. Cagigal and V. F. Canales, "Photon statistics in partially compensated wave fronts," *J. Opt. Soc. Am. A*, 16, 2550-2554 (1999).
11. C. Aime and R. Soummer, "The usefulness and limits of coronagraphy in the presence of pinned speckles," *Astrophys.J.*, 612, L85-L88 (2004).
12. D. T. Gavel, J. R. Morris, R. G. Vernon, "Systematic design and analysis of laser-guide-star adaptive-optics systems for large telescopes," *J. Opt. Soc. Am. A*, 11, 914-924 (1994).
13. S. S. Olivier, J. An, K. Avicola, et al, "Performance of adaptive optics at Lick Observatory," *Proc. SPIE*, 2201, 1110-1120 (1994).
14. D. T. Gavel, E. L. Gates, C. E. Max, et al, "Recent science and engineering results with the laser guidestar adaptive optics system at Lick Observatory," *Proc. SPIE* 4839, 354-359 (2003).
15. D. L. Walters and W. L. Bradford, "Measurements of r_0 and θ_0 : two decades and 18 sites," *Appl. Opt.* 36, 7876-7886 (1997).
16. C. B. Markwardt, <http://cow.physics.wisc.edu/~craigm/idl/fitting.html>
17. G. K. Kanji, *100 Statistical Tests*, SAGE Publications, 1999.
18. R. J. Scaddan and J. G. Walker, "Statistics of stellar speckle patterns," *Appl. Opt.*, 17, 3779-3784 (1978).